

## Article

# Transparent Conductive Indium Zinc Oxide Films: Temperature and Oxygen Dependences of the Electrical and Optical Properties

Akhmed K. Akhmedov<sup>1</sup>, Eldar K. Murliev<sup>1</sup>, Abil S. Asvarov<sup>2,\*</sup> , Arsen E. Muslimov<sup>2</sup>   
and Vladimir M. Kanevsky<sup>2</sup>

<sup>1</sup> Institute of Physics, Dagestan Research Center of Russian Academy Sciences, Yaragskogo Str., 94, 367015 Makhachkala, Russia

<sup>2</sup> Shubnikov Institute of Crystallography, Federal Scientific Research Center “Crystallography and Photonics” of Russian Academy of Sciences, Leninsky Prospect, 59, 119333 Moscow, Russia

\* Correspondence: abil-as@list.ru

**Abstract:** Achieving high-efficiency optoelectronic devices often requires the development of high transparency in the extended range and high-conductivity materials, which can be ensured by the high mobility of charge carriers being used as the electrode. Among the candidate materials, transparent conductive indium zinc oxide (IZO) has attracted significant interest because of its superior electron mobility ( $5\text{--}60\text{ cm}^2/\text{V}\cdot\text{s}$ ) and the thermal stability of its structure. In this study, the IZO films were deposited by the radio frequency magnetron sputtering of the IZO ceramic target (containing 10 wt.% ZnO) by varying the two variables of the substrate temperature and the oxygen content in the working gas. Here, the importance of the deposition of the IZO films at a low substrate temperature, not exceeding  $100\text{ }^\circ\text{C}$ , in order to get the minimum values of the film resistivity is revealed. At a substrate temperature of  $100\text{ }^\circ\text{C}$ , the film deposited in pure argon demonstrated a minimum resistance of  $3.4 \times 10^{-4}\ \Omega\cdot\text{cm}$ . Despite the fact that, with the addition of  $\text{O}_2$  in the working gas, an increase in resistivity was observed, the IZO film that deposited under 0.4%  $\text{O}_2$  content demonstrated the highest mobility ( $\mu = 35\text{ cm}^2/\text{V}\cdot\text{s}$  at  $\rho = 6.0 \times 10^{-4}\ \Omega\cdot\text{cm}$ ) and enhanced transparency in the visible (VIS,  $400\text{--}800\text{ nm}$ ) and near-infrared (NIR,  $800\text{--}1250\text{ nm}$ ) ranges ( $T_{\text{VIS}} \geq 77\%$  and  $T_{\text{NIR}} \geq 76\%$ ). At an oxygen content above 0.4%, a significant deterioration in electrical properties and a decrease in optical characteristics were observed. SEM and XRD studies of the microstructure of the IZO films allowed the clarification of the effect of both the substrate temperature and the oxygen content on the functional characteristics of the transparent conducting IZO films.

**Keywords:** TCO; thin films; indium zinc oxide; transparent electrode; magnetron sputtering; mobility; transmittance



**Citation:** Akhmedov, A.K.; Murliev, E.K.; Asvarov, A.S.; Muslimov, A.E.; Kanevsky, V.M. Transparent Conductive Indium Zinc Oxide Films: Temperature and Oxygen Dependences of the Electrical and Optical Properties. *Coatings* **2022**, *12*, 1583. <https://doi.org/10.3390/coatings12101583>

Academic Editors: Panos Pouloupoulos and Andrey V. Osipov

Received: 30 September 2022

Accepted: 18 October 2022

Published: 19 October 2022

**Publisher's Note:** MDPI stays neutral with regard to jurisdictional claims in published maps and institutional affiliations.



**Copyright:** © 2022 by the authors. Licensee MDPI, Basel, Switzerland. This article is an open access article distributed under the terms and conditions of the Creative Commons Attribution (CC BY) license (<https://creativecommons.org/licenses/by/4.0/>).

## 1. Introduction

Transparent conductive oxide films (TCO films), due to their high transmittance and low resistivity, have been extensively used as electrodes in various optoelectrical devices, including photovoltaic solar cell [1,2], flat panel display [3], light-emitting diodes [4–6], sensors [7], etc. Conventional TCO materials, such as  $\text{In}_2\text{O}_3:\text{Sn}$  (ITO), highly doped ZnO (with Ga, Al, In, B, etc.) and  $\text{SnO}_2:\text{F}$ , are steadily under study and have been widely utilized in the device industry [1,2,6,8–10]. However, a critical problem in achieving good electrical performance for these materials is an unavoidable high-temperature process in order to activate dopants by substrate heating up to  $300\text{ }^\circ\text{C}$  directly during film deposition or during subsequent postannealing, which severely limits their application in the dynamically developing area of optoelectronic devices on organic flexible substrates, also called flexible and stretchable optoelectronics [7,11]. A boom in interest in recently emerging fields, such as flexible display using organic light-emitting diodes (OLED) and tandem solar

cells stacked with perovskite and Cu(In,Ga)Se<sub>2</sub> (CIGS), has led to new requirements for transparent electrodes. For OLED application, the control of the film microstructure and the film surface roughness associated with it, as well as the adjustment of the electrode work function, come to the fore [12,13]. In turn, the widening of the transparency window of the TCO electrode to the NIR region, while maintaining its good electrical performance, is one of the most important tasks applied to CIGS-based solar cells [14–16].

Currently, an indium zinc oxide system is one of the more promising materials for TCO films due to its high transmittance, good electrical properties, thermal stability and lowest deposition temperature. Moreover, a tunable work function, high etching rate, smoother surface and resistance to moist heat are the prominent features of IZO thin films, which are very important aspects for OLED display applications [13,17]. Regarding the use of IZO films as transparent electrodes in tandem solar cells, a very important fact is the opportunity to achieve a much lower NIR absorption due to their low charge-carrier density, which is compensated by their exceptionally high electron mobility that simultaneously allows for a high conductivity [16,18,19].

IZO thin films with varying compositions have been deposited by various deposition technologies, such as sputtering [13,16,17,19], pulsed laser deposition [20], thermal evaporation [21], atomic layer deposition [22] and wet-solution process [23].

Among them, sputtering is the most established deposition technique due to its great advantages, such as a high deposition rate, high-quality film and simple scalability to large deposition areas [8,24], despite the fact that it can lead to plasma damage, resulting in degradation of the device's performance. Sufficient studies have been devoted to achieving good electrical properties while maintaining high optical transmittance through optimizing magnetron sputtering conditions [17,19,25–30]. Initially, studies focused on the effects of the specific doping concentration [25,30], oxygen partial pressure [19,29] and temperature regime [17,28] on the functional properties of the IZO films. Often, the results obtained differed from each other due to the peculiarities of the growth conditions in a particular experiment.

In this study, we are going to explore the effects of the two key important variables of the substrate temperature and the oxygen content in the working gas on the final functional properties of the IZO (In<sub>2</sub>O<sub>3</sub> with 10 wt.% ZnO) films by using a magnetron sputtering setup, which had been equipped with a specially designed multi-position drum-type substrate holder [31]. The substrate holder allows for quick growth temperature optimization for different materials due to the simultaneous growth of films on substrates at different controlled temperatures in a single vacuum run [31,32], i.e., for each value of the oxygen content, a set of IZO thin-film samples differing from each other only in the deposition temperature will be obtained simultaneously.

## 2. Materials and Methods

### 2.1. IZO Thin Films Synthesis

A series of IZO films were fabricated by the radio frequency (rf) magnetron sputtering of an IZO ceramic target (90 wt.% In<sub>2</sub>O<sub>3</sub> and 10 wt.% ZnO) on soda-lime glass slides (25 × 25 × 1.1 mm) at substrate temperatures of room temperature (RT), 100, 200 and 300 °C under different contents of oxygen  $c(\text{O}_2)$  in an Ar-based working gas mix (from 0.0 to 2.0%).

The IZO ceramic target in the form of a 2-inch disk was synthesized as follows. Submicron powders of In<sub>2</sub>O<sub>3</sub> (99.99% purity) and ZnO (99.95% purity) under a weight ratio of 9:1 were used as a starting powder mix. The powder mixture was successively subjected to 5 h of dry mixing in a ball mill, 8 h of annealing in air at 900 °C and repeated 5 h of processing in a ball mill. Then, the prepared powder mix was used to form a ceramic disc with a diameter of 51 mm and a thickness of 4 mm using the spark plasma sintering (SPS) technique [33] under the SPS temperature of 950 °C and SPS duration of 5 min. After mechanical grinding, the ceramic disk was finally annealed in air at 900 °C for 2 h.

A home-made rf magnetron sputtering setup provided pumping down to a base pressure of lower than  $2 \times 10^{-4}$  Pa and was equipped with a multiposition drum-type heated substrate holder, which ensured the simultaneous formation of four films at different temperatures (from room temperature to 300 °C) in one vacuum cycle [31]. To study the effects of the oxygen, pure argon ( $c(\text{O}_2) = 0.0\%$ ) and preliminarily prepared Ar/O<sub>2</sub> working gas mixes (with varying  $c(\text{O}_2)$  from 0.3 to 2.0%) were used. For each  $c(\text{O}_2)$ , four thin-film samples were deposited in a single vacuum cycle at four values of substrate temperatures under the following deposition conditions: the sputtering pressure of 0.5 Pa at a flow rate of 20 sccm, the rf power of 100 W, the rotation rate of the drum substrate holder of 10 rpm (the minimum distance from the target to the passing substrate was 100 mm), and a sputtering duration of 200 min.

## 2.2. IZO Film Characterization

The sheet resistance of the IZO thin films was measured by using a four-point technique (IUS-3, Moscow, Russia), while electrical transport properties were characterized from Hall effect measurements at room temperature by using the van der Pauw geometry. The optical transmittance of the IZO thin films coated on glass substrates was recorded by an optical spectrophotometer (Shimadzu UV-3600, Tokio, Japan) in the wavelength range of 300–1250 nm.

The films' thickness was evaluated from transmission spectra by using the PUMA approach and code described by Birgin et al. [34] and confirmed by scanning electron microscopy measurements (SEM, Leo-1450, Carl Zeiss, Oberkochen, Germany).

A scanning electron microscopy method was also used to observe both the cross-sectional and surface morphology of the deposited films, while an XRD method in  $\theta$ -2 $\theta$  scan mode was used to determine their structural characterization (Shimadzu XRD-7000, Tokio, Japan).

## 3. Results and Discussion

Figure 1 shows the deposition rate of the IZO thin films prepared under varying oxygen concentrations  $c(\text{O}_2)$ . In this figure, each node of the curve corresponds to the average value measured on the four films deposited at substrate temperatures ranging from room temperature to 300 °C. The deposition rate increased until an  $c(\text{O}_2)$  of 0.3% in the working gas mix was reached, while it noticeably decreased with the further increasing of oxygen concentration in the O<sub>2</sub>/Ar gas mix. The increase in the growth rate observed at a low oxygen content may be due to the formation of a metal-rich condition in the IZO target during its preparation by the SPS method [35]. The addition of a small amount of oxygen should promote the oxidation of both surplus Zn and hemioxide In<sub>2</sub>O, which, if sputtered in an inert atmosphere, can relatively easily resputter from the exposed surface due to high vapor pressure. Full oxidation of sputtered species results in a higher deposition rate. In turn, the decrease in the deposition rate with an increase in the oxygen content above 0.3% resulted in both the formation of a thin oxidized layer on the surface of the IZO target under the oxygen ambient in the chamber and the decrease of Ar ions bombarding the target surface [29].

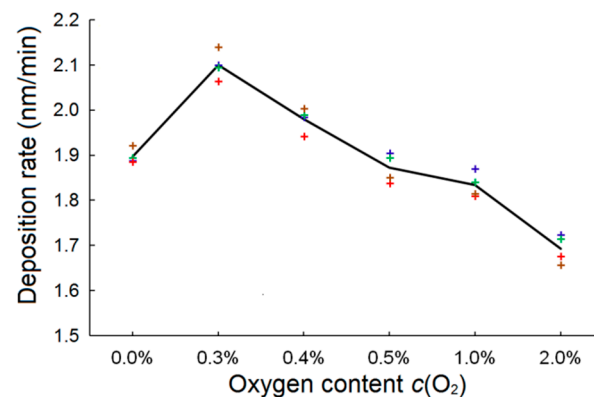
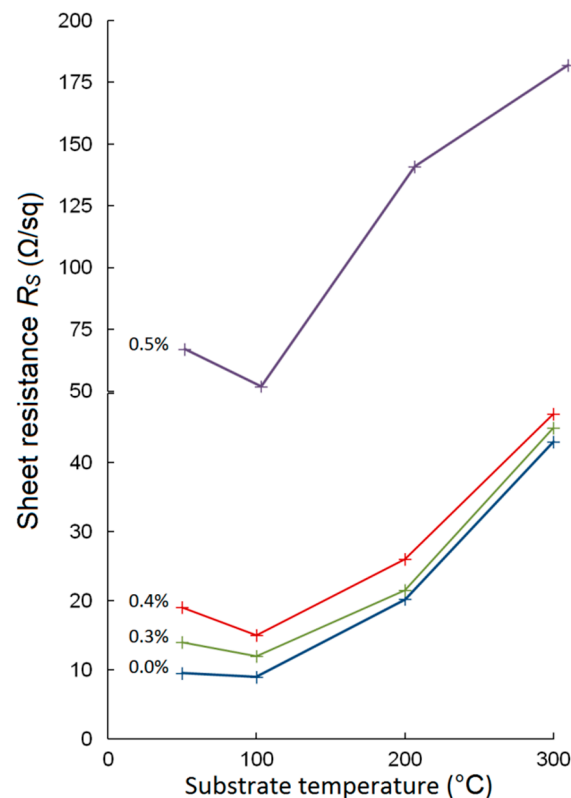


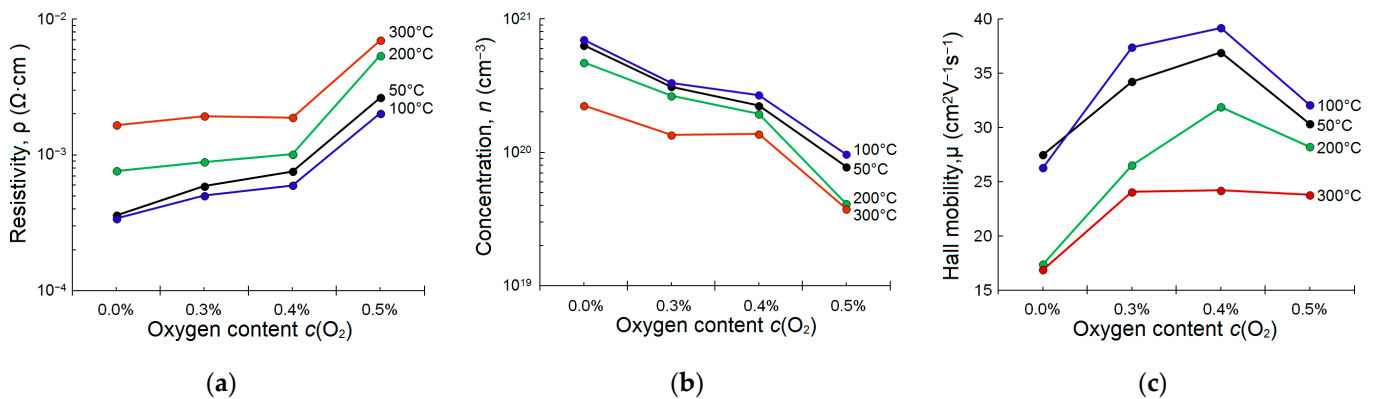
Figure 1. Deposition rate of the IZO thin films deposited under varying oxygen contents.

Figure 2 shows the changes in sheet resistance  $R_S$  of the IZO films deposited at an  $O_2$  content up to 0.5% as a function of the substrate temperature during deposition. In Figure 2, there are no data corresponding to the IZO films deposited at an  $O_2$  content of 1 and 2%, due to the fact that these films had high values of sheet resistance ( $R_S > 10^5 \Omega/\text{sq}$ ) that are far from the acceptable TCO resistance requirement. Figure 2 shows that, for each  $c(O_2)$ , the sheet resistance of the IZO films decreased quite a bit with the increasing of the substrate temperature from RT to 100 °C, while a further increase in the substrate temperature leads to an increase in resistance by several times. This result indicates that IZO, unlike more traditional TCO materials (ITO, doped ZnO, etc.) [31,32], does not require high temperature substrate heating, as has been noted previously by many groups [13,16,19].



**Figure 2.** Sheet resistance  $R_S$  of the IZO films deposited under the oxygen content  $c(O_2)$  from 0.0 to 0.3% as a function of the substrate temperature.

In order to gain more information about the aspects leading to this IZO behavior, direct measurements of the electrical properties of the IZO thin films deposited at the various substrate temperatures were performed using the Hall Effect technique. Figure 3 shows the dependences of the resistivity  $\rho$ , the Hall mobility  $\mu$  and the carrier concentration  $n$  as a function of the oxygen concentration  $c(O_2)$ . It can be seen that, for the range of  $O_2$  content studied, the minimum values of resistivity  $\rho$  were observed in the IZO films deposited at the substrate temperature of 100 °C (Figure 3a), as in the case of the dependence of sheet resistance on substrate temperatures (Figure 2). At the same time, as observed in Figure 3a, for each substrate temperature, there is a tendency for  $\rho$  to rise with the increase in the  $c(O_2)$ —a minor change in the  $\rho$  at an  $c(O_2)$  of less than 0.4% and a sharp increase above an  $c(O_2)$  of 0.4%.



**Figure 3.** Electrical properties of the IZO thin films deposited at the various substrate temperatures as a function of the oxygen content  $c(O_2)$ : (a) Data for the resistivity  $\rho$ ; (b) Data for the carrier concentration  $n$ ; (c) Data for the Hall mobility  $\mu$ .

This effect occurs due to the competing trends of  $n$  and  $\mu$  (Figure 3b,c). For example, in the case of a substrate temperature of 100 °C, the  $n$  decreases with the increasing of the  $c(O_2)$ , from  $6.7 \times 10^{20}$  down to  $1 \times 10^{20} \text{ cm}^{-3}$ , while the  $\mu$  has a prominent maximum of  $39.2 \text{ cm}^2/\text{V} \cdot \text{s}$  for  $c(O_2) = 0.4\%$ . The films deposited at 50, 200 and 300 °C follow the same trend.

Thus, in the course of a comparative study of the electrical characteristics of the IZO films as functions of the substrate temperature and the  $O_2$  concentration, the following was found:

- In order to achieve the minimal values of resistivity in the IZO films, it was necessary to carry out sputtering at a substrate temperature not exceeding 100 °C;
- At this substrate temperature, the mobility could be increased from 25 to more than  $37 \text{ cm}^2/\text{V} \cdot \text{s}$  by adding up to 0.4%  $O_2$  to the working gas Ar. At the same time, despite the concomitant slight decrease in the carrier concentration from  $6.7 \times 10^{20}$  to  $2.7 \times 10^{20} \text{ cm}^{-3}$ , the deposited films were characterized by resistivity values  $\rho \leq 6 \times 10^{-4} \Omega \cdot \text{cm}$  (which corresponds to a sheet resistance  $R_S$  less than  $15 \Omega/\text{sq}$  at the films' thickness of 400 nm), meeting conventional TCO requirements;
- When using substrate temperatures and oxygen concentrations above optimal values (100 °C and 0.4%  $O_2$ , respectively), a noticeable downgrade of electrical performance in IZO is observed due to a decrease in both the concentration and mobility.

The normal-incidence transmission spectra of a glass substrate with the IZO thin films were measured by the optical spectrophotometry in the 300–1250 nm wavelength range. Figure 4a displays the optical transmittance of the IZO films deposited in the pure Ar working gas with varying substrate temperatures.

The data showed distinct interference fringes indicating that the films were smooth with little scatter. Figure 4a shows that the transparency of the IZO films deposited in pure Ar was increased in the visible range (400–800 nm) with increased substrate temperatures. This may be due to a decrease in the photon absorbance and scattering on defects caused by the incorporation of surplus metals into the film. At the same time, the transmittance of the films in the NIR region (800–1250 nm), as a function of substrate temperatures, repeats the trend of the concentration  $n$  in the films with varying substrate temperatures. The minimum transparency in this region was shown by the film deposited at 100 °C, which had the maximum concentration  $n = 6.9 \times 10^{20} \text{ cm}^{-3}$  among the films deposited at an  $c(O_2)$  of 0.0%.

Figure 4b illustrates the optical transmittance spectra of the IZO films deposited at the substrate temperature of 100 °C with varying oxygen concentrations in the working gas. The films deposited at an  $c(O_2)$  of 0.3–0.4% present maximum transparency (the average transmittance  $\bar{T}_{VIS}$  calculated in the visible range of 400–800 nm for these films was more than 77%), while below and above the  $c(O_2)$  the average transmittance  $\bar{T}_{VIS}$  slightly drops (73.5 and 75.8%, respectively). The decrease in the  $\bar{T}_{VIS}$  with an increase in the  $c(O_2)$  to 0.5% is mainly due to a dip in the spectrum in the violet-blue region (380–470 nm). Regarding

the NIR region, all three films deposited in the presence of  $O_2$  are characterized by a high transparency in this range compared to the film deposited at an  $c(O_2) = 0\%$ . Note that a clearer picture of the absorption edge red shift with an increasing  $c(O_2)$  is observed in the spectral vicinity of 350 nm for the IZO films deposited at 100 °C. That can be attributed to the well-known Burstein–Moss shift due to the observed increase in the concentration  $n$  by almost one order of magnitude with a decreasing  $c(O_2)$  from 0.5 to 0.0%.

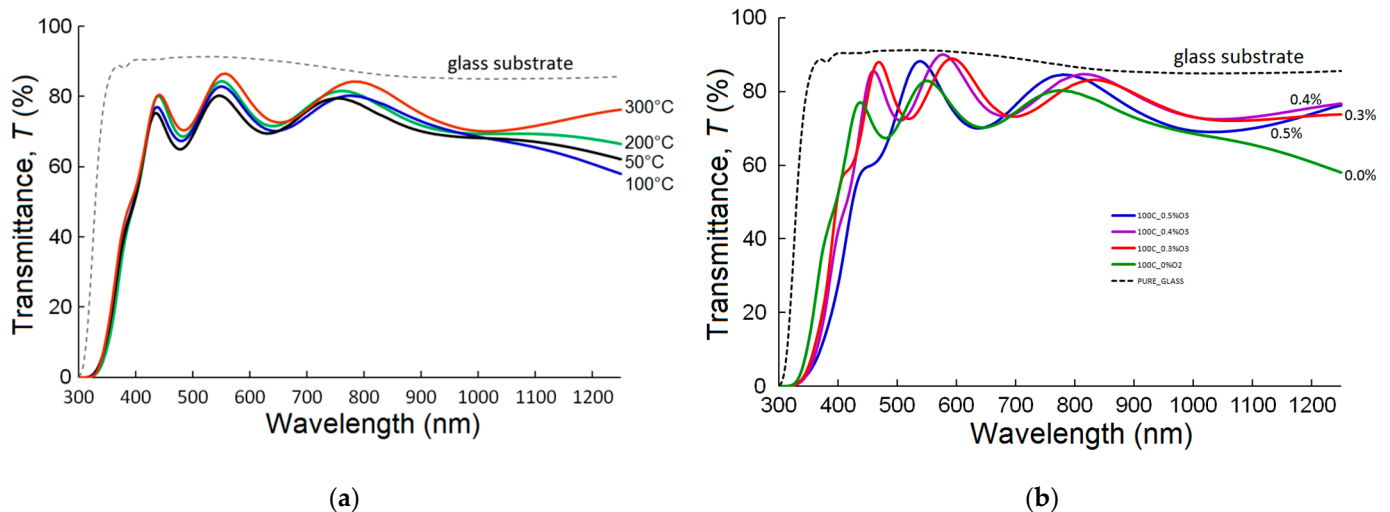


**Figure 4.** (a) Optical transmittance of the IZO films deposited in pure Ar with varying substrate temperatures; (b) Optical transmittance of the IZO films deposited at substrate temperatures of 100 °C with varying oxygen contents  $c(O_2)$ .

The average transmittances  $\bar{T}_{VIS}$  and  $\bar{T}_{NIR}$  calculated for the visible (400–800 nm) and NIR (800–1250 nm) regions, depending on the substrate temperature and  $c(O_2)$ , are also summarized in Figure 5a,b, respectively. It can be seen from Figure 5a that, while the average transmittance  $\bar{T}_{VIS}$  of the films deposited at an  $c(O_2)$  of 0.0 and 0.5% show opposite direction dependences with varying substrate temperatures, the dependences of the  $\bar{T}_{VIS}$  on the substrate temperature for the IZO films deposited at the intermediate  $c(O_2)$  values (0.3% and 0.4%) are less pronounced. Note that the maximum average transmittance in these films ( $\bar{T}_{VIS} = 77.5\%$ ) is achieved in the substrate temperature range of 100–200 °C. Taking into account the slightly larger film thickness obtained by an  $c(O_2) = 0.3\%$ , we can conclude that the IZO thin film deposited at 100 °C and an  $O_2$  content of 0.3% demonstrates maximum transparency in the visible area. In turn, the IZO film obtained at 100 °C and an  $c(O_2) = 0.4\%$ , in which the maximum mobility was observed, is characterized by the maximum transmittance in the NIR region ( $\bar{T}_{NIR} = 76.4\%$ ) among all the films (Figure 5b).

Thus, the transmittance for the glass substrate with the IZO thin films showed that the adding of  $O_2$  in the working gas clearly leads to a red shift in the optical response for the UV-violet region. However, for wavelengths greater than 400 nm, the transmittance values increased, reaching values greater than 76% of transparency in the wide visible–NIR range for the IZO films deposited at the optimal substrate temperature (100 °C) and the  $c(O_2)$  values up to 0.4%. A further increase in the  $c(O_2)$ , especially in combination with an increase in the substrate temperature, leads to a substantial decrease in the average transmittance.

On the whole, based on the regularities observed in the study of the electrical and optical properties of the IZO films, it can be concluded that this behavior is characteristic of mostly amorphous  $In_2O_3$ -based thin films, in which the conductivity is governed mainly by oxygen vacancies [36–38]. In this regard, the resistance of the IZO films could be controlled and easily changed by nine orders of magnitude [39]. Furthermore, we also noted that, in our experiment, the IZO films that deposited at an  $c(O_2) \geq 1\%$  had high values of resistivity, beyond the measurement limits of our measurement setup. In turn, it has been demonstrated that the deposition of the IZO film under a controlled low oxygen content

in a chamber allows the fine-tuning of both the electrical and optical properties of these thin films by enhancing the mobility of the IZO film due to the decrease in concentration of  $V_O$  in the film [19,29]. Kamiya et al. suggested, on the basis of first-principles calculations, that oxygen vacancies ( $V_O$ ) act as shallow donors and suppliers of conduction electrons in amorphous  $\text{In}_2\text{O}_3$ -containing thin films, and that defect sites, meanwhile, can also act as scattering centers, reducing charge-carrier conduction [40].

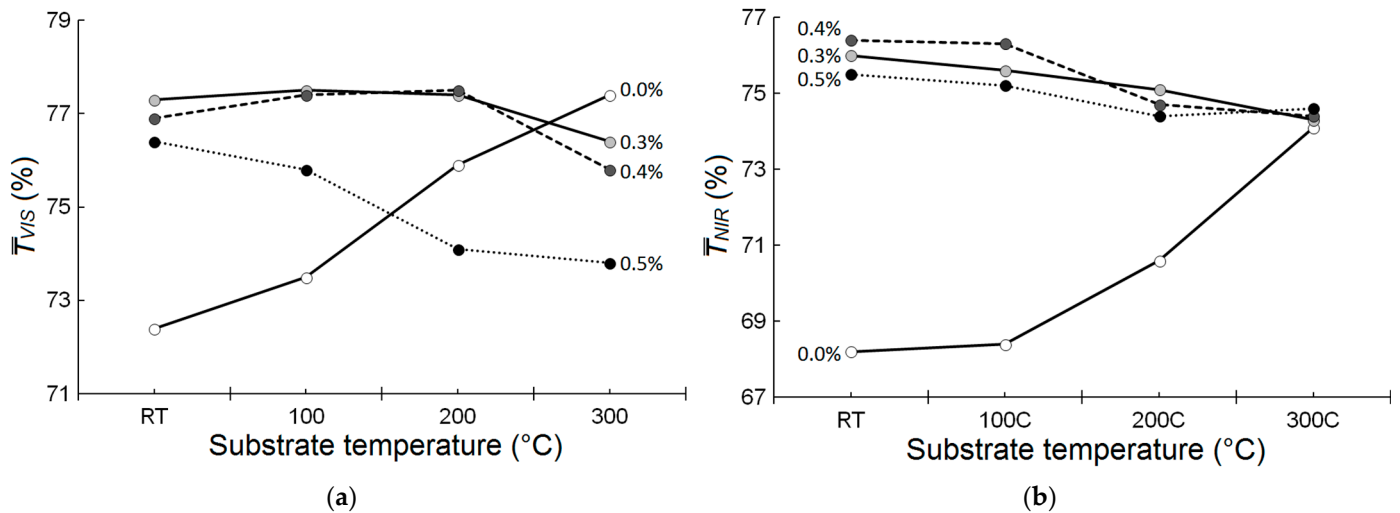


**Figure 5.** (a) Average transmittance  $\bar{T}_{\text{VIS}}$  of the IZO films deposited under the various  $c(\text{O}_2)$  as a function of the substrate temperatures; (b) Average transmittance  $\bar{T}_{\text{NIR}}$  of the IZO films deposited under the various  $c(\text{O}_2)$  as a function of the substrate temperatures.

Based on our measurement data on the electrical characteristics of the IZO films, we plotted the dependence of  $\mu$  with  $n$  (Figure 6). The ramp and subsequent decrease of  $\mu$  with  $n$  could be explained by the presence of different scattering mechanisms. According to Leenheer et al., the maximum  $\mu$  in the IZO films is reached when carrier transport is mainly limited by phonon scattering, i.e., metal-like transport [41]. The change in trend observed on the curves in Figure 6 may indicate that ionized impurity scattering becomes the main limiting factor of  $\mu$  at a high concentration of carriers supplied by  $V_O$ . The values of the  $n$ , at which the scattering mechanism switches, are in agreement with [19,41]. Here, it is worth noting that a change in the location of the maximum of the curves depending on the substrate temperature may indicate the presence of some additional mechanisms of charge-carrier scattering. In particular, due to the nonstoichiometric nature of the sputtered target, the formation of metal pairs (e.g., In-In, In-Zn), and even subnanometer metal inclusions, is possible inside the film at RT [42,43]. These defects can be additional scattering centers for both conduction electrons and transmitted light. With increasing substrate temperatures, the formation of metal inclusions is reduced and the mobility of the films improves. This can explain the improvement in both the electrical and optical properties of the IZO films observed in our experiment with an increase in the substrate temperature from RT to 100 °C.

Furthermore, since the IZO films deposited at an optimal substrate temperature of 100 °C under the oxygen ambient have a higher transparency than the IZO films deposited at 300 °C under the same ambient (which is not in agreement with others [28]), we carried out additional comparative studies of the morphology and microstructure of the corresponding IZO films.

Figure 7 shows the SEM micrographs of the IZO thin films deposited at a substrate temperature of 100 and 300 °C by using the various oxygen contents in the working gas. It is shown that a very flat surface was obtained at a low substrate temperature regardless of the  $c(\text{O}_2)$ . Such morphology is typical in the case of the kinetic regime of the deposition of a multicomponent oxide film, the individual components of which have

minimal solubilities in each other [13,36]. In this case, the absence of any significant external heating of the growing film usually results in the formation of a closely packed homogeneous amorphous/nanocrystalline structure.

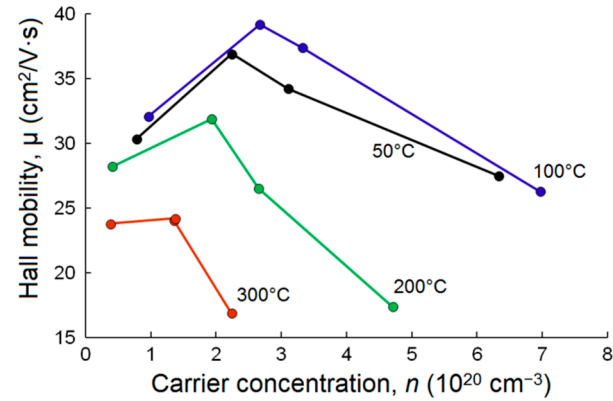


Figure 6. The dependence of  $\mu$  with  $n$ .

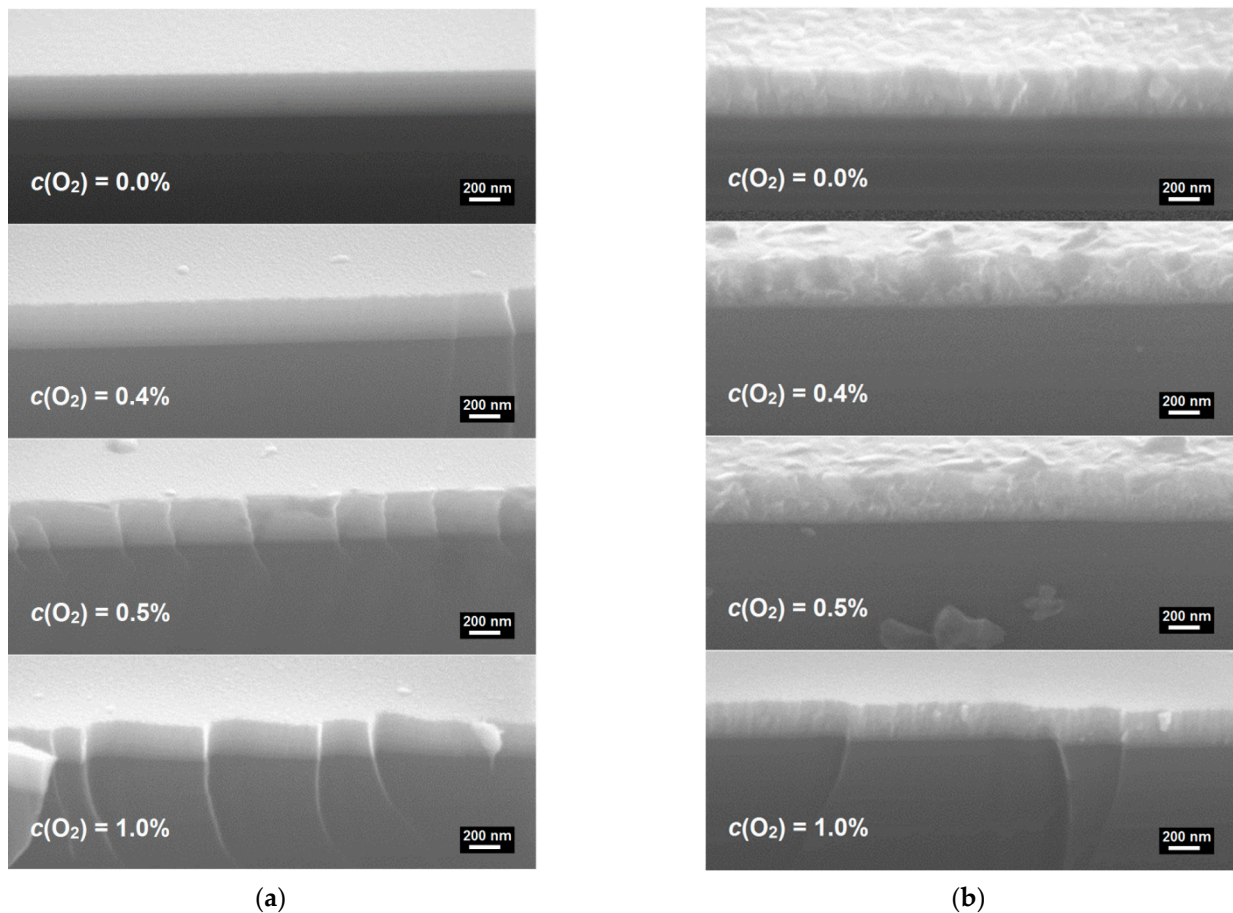


Figure 7. SEM morphology images of the IZO films deposited under various  $c(\text{O}_2)$  at the substrate temperatures of 100 (a) and 300 °C (b).

In contrast, the surface roughness of the IZO films deposited at 300 °C and an  $c(\text{O}_2)$  range up to 0.5% is greatly increased in comparison with that of the IZO films deposited at the optimal 100 °C. The film deposited in pure argon had signs of columnarity. The formation of a columnar structure is typical, for example, for polycrystalline ITO films grown on a heated substrate [44]. When the  $c(\text{O}_2)$  increased up to 0.5%, the surface became

more rough and highly disordered grains appeared locally. Note that, when the  $c(\text{O}_2)$  became greater than 0.5%, the surface of the film became very smooth, like that of the films deposited at a lower substrate temperature. The complex behavior of the morphology in the IZO films deposited at 300 °C is related, apparently, to the oppositional nature of the effect of oxygen on the growth of ZnO and  $\text{In}_2\text{O}_3$ , whose nanocrystals (nanoclusters) can nucleate inside the film at a given temperature [35,45,46].

Thus, SEM studies have revealed the relationship between the deterioration in light transmission observed for films deposited at temperatures above 100 °C (Figure 4) and the development in their surface morphology. It is well-known that, during optical transmittance measurement, the incident light can be more scattered over a rough surface than over a uniform surface [47].

Figure 8 shows the x-ray diffraction spectra obtained from the IZO thin films deposited at 100 and 300 °C and various  $c(\text{O}_2)$ . XRD studies confirmed the most common amorphous nature of the films of the indium zinc oxide system, except the IZO film deposited in pure Ar at 300 °C. All the samples prepared at a low substrate temperature show no clear or broad diffraction peaks, which indicate that these films were fully disordered due to the immiscibility of Zn in the  $\text{In}_2\text{O}_3$  matrix. A somewhat different picture was observed in the case of substrate temperatures of 300 °C. For the film deposited at 300 °C in pure Ar, a clear peak indicates the presence of polycrystalline IZO. Its position is very close to the position of the diffraction (222) line for  $\text{In}_2\text{O}_3$  (PDF card #00-006-0416). At the same time, with the addition of oxygen, ordering transformation occurs on the patterns of the IZO films deposited at 300 °C. For the film deposited at an  $c(\text{O}_2) = 0.4\%$ , on the pattern there is only a weak and broad peak centered at  $2\theta = 30^\circ$ , indicating that the film is an amorphous structure with some short-range ordering. However, this broad peak does not exclude the possibility of the presence of ultrafine crystallites of oxide phases (In-doped ZnO, Zn-doped  $\text{In}_2\text{O}_3$ , and other compounds from the homologous series  $\text{In}_2\text{Zn}_k\text{O}_{k+3}$ ) into the film, the size of which does not exceed a few nanometers [48,49]. In the end, more complete amorphization is observed with an increasing  $c(\text{O}_2)$  up to 1%.

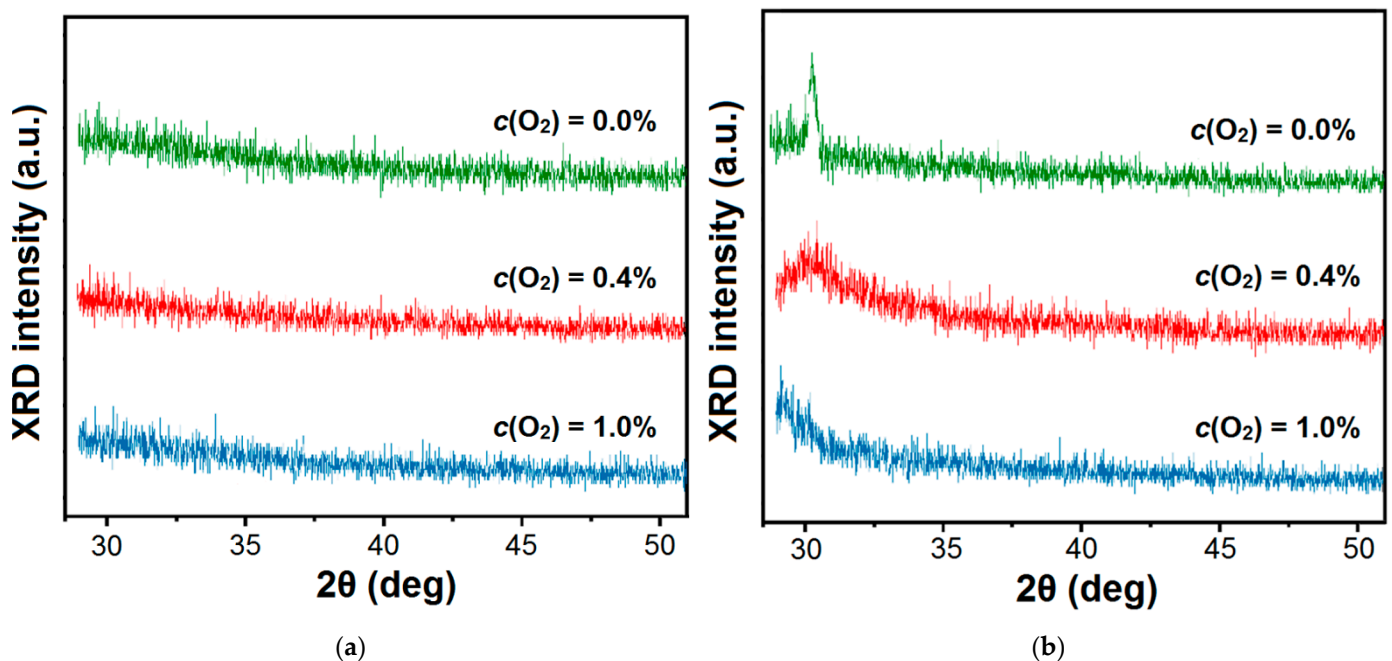


**Figure 8.** XRD patterns from the IZO films deposited under various  $c(\text{O}_2)$  at the substrate temperatures of 100 (a) and 300 °C (b).

#### 4. Conclusions

The functional characteristics of the IZO TCO thin films prepared by the rfmagnetron sputtering of the SPS synthesized ceramic IZO target (90 wt.% In<sub>2</sub>O<sub>3</sub> and 10 wt.% ZnO) were well investigated in this study. We have shown the influence on the carrier-transport properties and optical transmittance of the oxygen partial pressure and substrate temperature applied during the sputtering deposition of the IZO thin films.

It is shown that the electrical properties behaved as if dominant donors are mainly generated by oxygen vacancies. Enhanced electrical property of the IZO films was achieved by decreasing the substrate temperature up to 100 °C, which showed a 9 Ω/sq of sheet resistance for the film with a thickness of about 380 nm obtained in pure Ar.

Despite the fact that, with an increase in the oxygen content, an increase in resistivity was observed, it was found that the addition of oxygen during sputtering differently affects the carrier concentration and its mobility. While the concentration decreased monotonically over the entire range of the oxygen content, the mobility had a maximum ( $\mu = 39.2 \text{ cm}^2/\text{V}\cdot\text{s}$ ) at an oxygen content of 0.4%. It has been demonstrated that, in films deposited at the optimal temperature, the addition of oxygen up to 0.4% also leads to an increase in transparency in both the visible and near-infrared regions of the spectrum ( $\bar{T}_{VIS} \geq 77\%$  and  $\bar{T}_{NIR} \geq 76\%$ ). Additional studies of the morphology and microstructure of the deposited films made it possible to identify the reasons for the observed deterioration of the optical properties of the IZO films deposited at non-optimal conditions.

In conclusion, the strategy to grow IZO film, based on the optimization of oxygen vacancies into IZO by O<sub>2</sub> introduced during sputtering, is a useful guideline for the tuning of the functional properties of low-temperature IZO TCO films and their adaptation for some practical applications, including a wide area of temperature-sensitive and flexible devices.

**Author Contributions:** Conceptualization, A.K.A. and A.S.A.; methodology, A.K.A.; validation, A.K.A., A.E.M. and A.S.A.; formal analysis, V.M.K.; investigation, E.K.M., A.K.A., A.S.A. and A.E.M.; resources, A.K.A. and V.M.K.; writing—original draft preparation, A.K.A. and A.S.A.; writing—review and editing, A.S.A. and V.M.K.; supervision, A.S.A. and V.M.K. All authors have read and agreed to the published version of the manuscript.

**Funding:** This research was performed in the frame of state assignments of Ministry of Science and Higher Education of the Russian Federation for Dagestan Federal Research Center of Russian Academy of Sciences and Federal Scientific Research Center “Crystallography and Photonics” of Russian Academy of Sciences.

**Institutional Review Board Statement:** Not applicable.

**Informed Consent Statement:** Not applicable.

**Data Availability Statement:** Not applicable.

**Acknowledgments:** The authors are grateful for additional technical support from the Analytical Shared Research Center of Dagestan Federal Research Center of RAS and the Shared Research Center of FSRC “Crystallography and Photonics” RAS.

**Conflicts of Interest:** The authors declare no conflict of interest.

#### References

1. Kim, Y.; Joo, S.H.; Shin, S.G.; Choi, H.W.; Bark, C.W.; Rim, Y.S.; Kim, K.H.; Kim, S. Effect of Annealing in ITO Film Prepared at Various Argon-and-Oxygen-Mixture Ratios via Facing-Target Sputtering for Transparent Electrode of Perovskite Solar Cells. *Coatings* **2022**, *12*, 203. [[CrossRef](#)]
2. Chen, P.-H.; Chen, W.-J.; Tseng, J.-Y. Thermal Stability of the Copper and the AZO Layer on Textured Silicon. *Coatings* **2021**, *11*, 1546. [[CrossRef](#)]
3. Kawajiri, K.; Tahara, K.; Uemiya, S. Lifecycle assessment of critical material substitution: Indium tin oxide and aluminum zinc oxide in transparent electrodes. *Resour. Environ. Sustain.* **2022**, *7*, 100047. [[CrossRef](#)]
4. Liang, S.; Zhou, Q.; Li, X.; Zhong, M.; Wang, H. Electrical and Optical Properties of a Transparent Conductive ITO/Ga<sub>2</sub>O<sub>3</sub>/Ag/Ga<sub>2</sub>O<sub>3</sub> Multilayer for Ultraviolet Light-Emitting Diodes. *Nanomaterials* **2019**, *9*, 403. [[CrossRef](#)] [[PubMed](#)]

5. Park, T.H.; Ren, W.; Lee, H.J.; Kim, N.; Son, K.R.; Rani, A.; Kim, T.G. Efficient TADF-based blue OLEDs with 100% stretchability using titanium particle-embedded indium zinc oxide mesh electrodes. *NPG Asia Mater.* **2022**, *14*, 66. [[CrossRef](#)]
6. Chen, Z.; Wang, J.; Wu, H.; Yang, J.; Wang, Y.; Zhang, J.; Bao, Q.; Wang, M.; Ma, Z.; Tress, W.; et al. A Transparent Electrode Based on Solution-Processed ZnO for Organic Optoelectronic Devices. *Nat. Commun.* **2022**, *13*, 4387. [[CrossRef](#)]
7. Kumar, N.; Arora, K.; Kumar, M. High performance, flexible and room temperature grown amorphous Ga<sub>2</sub>O<sub>3</sub> solar-blind photodetector with amorphous indium-zinc-oxide transparent conducting electrodes. *J. Phys. D Appl. Phys.* **2019**, *52*, 335103. [[CrossRef](#)]
8. Cheng, Y.-T.; Lu, T.-L.; Hong, M.-H.; Ho, J.-J.; Chou, C.-C.; Ho, J.; Hsieh, T.-P. Evaluation of Transparent ITO/Nano-Ag/ITO Electrode Grown on Flexible Electrochromic Devices by Roll-to-Roll Sputtering Technology. *Coatings* **2022**, *12*, 455. [[CrossRef](#)]
9. Wang, J.; Zou, X.; Zhu, J.; Cheng, J.; Chen, D.; Bai, X.; Yao, Y.; Chang, C.; Yu, X.; Liu, B.; et al. Effect of Optimization of TiO<sub>2</sub> Electron Transport Layer on Performance of Perovskite Solar Cells with Rough FTO Substrates. *Materials* **2020**, *13*, 2272. [[CrossRef](#)]
10. Jeong, S.-J.; Kim, K.-H.; Ahn, H.-J. Net-Patterned Fluorine-Doped Tin Oxide to Accelerate the Electrochromic and Photocatalytic Interface Reactions. *Catalysts* **2021**, *11*, 249. [[CrossRef](#)]
11. Hou, W.; Liao, Q.; Xie, S.; Song, Y.; Qin, L. Prospects and Challenges of Flexible Stretchable Electrodes for Electronics. *Coatings* **2022**, *12*, 558. [[CrossRef](#)]
12. Park, S.-R.; Suh, M.C. Enhanced device performances of a new inverted top-emitting OLEDs with relatively thick Ag electrode. *Opt. Express* **2018**, *26*, 4979–4988. [[CrossRef](#)] [[PubMed](#)]
13. Goncalves, G.; Grasso, V.; Barquinha, P.; Pereira, L.; Elamurugu, E.; Brignone, M.; Martins, R.; Lambertini, V.; Fortunato, E. Role of Room Temperature Sputtered High Conductive and High Transparent Indium Zinc Oxide Film Contacts on the Performance of Orange, Green, and Blue Organic Light Emitting Diodes. *Plasma Process. Polym.* **2011**, *8*, 340–345. [[CrossRef](#)]
14. Bush, K.A.; Bailie, C.D.; Chen, Y.; Bowring, A.R.; Wang, W.; Ma, W.; Leijtens, T.; Moghadam, F.; McGehee, M.D. Thermal and Environmental Stability of Semi-Transparent Perovskite Solar Cells for Tandems Enabled by a Solution-Processed Nanoparticle Buffer Layer and Sputtered ITO Electrode. *Adv. Mater.* **2016**, *28*, 3937–3943. [[CrossRef](#)] [[PubMed](#)]
15. Jošt, M.; Bertram, T.; Koushik, D.; Marquez, J.A.; Verheijen, M.A.; Heinemann, M.D.; Köhnen, E.; Al-Ashouri, A.; Braunger, S.; Lang, F.; et al. 21.6%-Efficient Monolithic Perovskite/Cu (In,Ga)Se<sub>2</sub> Tandem Solar Cells with Thin Conformal Hole Transport Layers for Integration on Rough Bottom Cell Surfaces. *ACS Energy Lett.* **2019**, *4*, 583–590. [[CrossRef](#)]
16. Schultes, M.; Helder, T.; Ahlswede, E.; Aygüler, M.F.; Jackson, P.; Paetel, S.; Schwenzler, J.A.; Hossain, I.M.; Paetzold, U.W.; Powalla, M. Sputtered Transparent Electrodes (IO:H and IZO) with Low Parasitic Near-Infrared Absorption for Perovskite–Cu (In,Ga)Se<sub>2</sub> Tandem Solar Cells. *ACS Appl. Energy Mater.* **2019**, *2*, 7823–7831. [[CrossRef](#)]
17. Rim, Y.S.; Kim, H.J.; Kim, K.H. Characteristics of indium zinc oxide films deposited using the facing targets sputtering method for OLEDs applications. *Thin Solid Film.* **2010**, *518*, 6223–6227. [[CrossRef](#)]
18. Calnan, S.; Tiwari, A.N. High mobility transparent conducting oxides for thin film solar cells. *Thin Solid Film.* **2010**, *518*, 1839–1849. [[CrossRef](#)]
19. Morales-Masis, M.; De Nicolas, S.M.; Holovsky, J.; De Wolf, S.; Ballif, C. Low-Temperature High-Mobility Amorphous IZO for Silicon Heterojunction Solar Cells. *IEEE J. Photovolt.* **2015**, *5*, 1340–1347. [[CrossRef](#)]
20. Socol, M.; Preda, N.; Stanculescu, A.; Breazu, C.; Florica, C.; Rasoga, O.; Stanculescu, F.; Socol, G. IZO deposited by PLD on flexible substrate for organic heterostructures. *Appl. Phys. A* **2017**, *123*, 371. [[CrossRef](#)]
21. Lee, W.-J.; Cho, D.-H.; Kim, Y.D.; Choi, M.-W.; Choi, J.C.; Chung, Y.-D. Thermally evaporated amorphous InZnO thin film applicable to transparent conducting oxide for solar cells. *J. Alloys Compd.* **2019**, *806*, 976–982. [[CrossRef](#)]
22. Lee, S.; Kang, Y.-H.; Kim, M.-S.; Lee, H.; Cho, Y.-H.; Kim, M.; Yoon, T.-S.; Kim, H.-M.; Kim, K.-B. Effect of the Bilayer Period of Atomic Layer Deposition on the Growth Behavior and Electrical Properties of the Amorphous In–Zn–O Film. *ACS Appl. Mater. Interfaces* **2020**, *12*, 39372–39380. [[CrossRef](#)] [[PubMed](#)]
23. Wang, L.; Liu, F.; Cai, X.; Ma, T.; Jiang, C. Indium Zinc Oxide Electron Transport Layer for High-Performance Planar Perovskite Solar Cells. *J. Phys. Chem. C* **2018**, *122*, 28491–28496. [[CrossRef](#)]
24. Kukla, R. Magnetron sputtering on large scale substrates: An overview on the state of the art. *Surf. Coat. Technol.* **1997**, *93*, 1–6. [[CrossRef](#)]
25. Minami, T.; Yamamoto, T.; Toda, Y.; Miyata, T. Transparent conducting zinc-co-doped ITO films prepared by magnetron sputtering. *Thin Solid Film.* **2000**, *373*, 189–194. [[CrossRef](#)]
26. Choi, Y.C.; Shin, H.J.; Han, D.C.; Ahn, K.-S.; Kim, J.H.; Lee, D.K. Transparent Zn-Doped In<sub>2</sub>O<sub>3</sub> Electrode Prepared by Radio Frequency Facing Target Sputtering for Flexible Dye-Sensitized Solar Cells. *Mol. Cryst. Liq. Cryst.* **2011**, *538*, 127–135. [[CrossRef](#)]
27. Jiang, H.; Wang, S.; Xu, Y.; Yang, S. Preparation of a-IZO thin films by RF magnetron sputtering for Cu (In, Ga) Se<sub>2</sub> solar cells. *J. Phys. Conf. Ser.* **2020**, *1549*, 042036. [[CrossRef](#)]
28. Kim, D.-G.; Lee, S.; Kim, D.-H.; Lee, G.-H.; Isshiki, M. Temperature dependence of the microstructure and resistivity of indium zinc oxide films deposited by direct current magnetron reactive sputtering. *Thin Solid Film.* **2008**, *516*, 2045–2049. [[CrossRef](#)]
29. Li, Y.L.; Lee, D.Y.; Min, S.R.; Cho, H.N.; Kim, J.; Chung, C.W. Effect of Oxygen Concentration on Properties of Indium Zinc Oxide Thin Films for Flexible Dye-Sensitized Solar Cell. *Jpn. J. Appl. Phys.* **2008**, *47*, 6896. [[CrossRef](#)]
30. Ishida, T.; Nishimura, T.; Chantana, J.; Mavlonov, A.; Kawano, Y.; Negami, T.; Minemoto, T. Tunable-Conduction-Band In–Zn–O-Based Transparent Conductive Oxide Deposited at Room Temperature. *Phys. Status Solidi A* **2022**, *219*, 2200061. [[CrossRef](#)]

31. Akhmedov, A.K.; Asvarov, A.S.; Muslimov, A.E.; Kanevsky, V.M. A Multi-Position Drum-Type Assembly for Simultaneous Film Deposition at Different Temperatures in a Single Sputter Cycle—Application to ITO Thin Films. *Coatings* **2020**, *10*, 1076. [[CrossRef](#)]
32. Asvarov, A.S.; Abduev, A.K.; Akhmedov, A.K.; Kanevsky, V.M. On the Effect of the Co-Introduction of Al and Ga Impurities on the Electrical Performance of Transparent Conductive ZnO-Based Thin Films. *Materials* **2022**, *15*, 5862. [[CrossRef](#)] [[PubMed](#)]
33. Asvarov, A.S.; Muslimov, A.E.; Akhmedov, A.K.; Abduev, A.K.; Kanevsky, V.M. A Laboratory Apparatus for Spark Plasma Sintering of Ceramic and Composite Materials. *Instrum. Exp. Tech.* **2019**, *62*, 726–730. [[CrossRef](#)]
34. Birgin, E.G.; Chambouleyron, I.; Martinez, J.M. Estimation of the Optical Constants and the Thickness of Thin Films Using Unconstrained Optimization. *J. Comput. Phys.* **1999**, *151*, 862–880. [[CrossRef](#)]
35. Akhmedov, A.; Abduev, A.; Murliev, E.; Asvarov, A.; Muslimov, A.; Kanevsky, V. The ZnO-In<sub>2</sub>O<sub>3</sub> Oxide System as a Material for Low-Temperature Deposition of Transparent Conductive Electrodes. *Materials* **2021**, *14*, 6859. [[CrossRef](#)]
36. Park, D.H.; Son, K.Y.; Lee, J.H.; Kim, J.J.; Lee, J.S. Effect of ZnO addition in In<sub>2</sub>O<sub>3</sub> ceramics: Defect chemistry and sintering behavior. *Solid State Ion.* **2004**, *172*, 431–434. [[CrossRef](#)]
37. Hosono, H. Ionic amorphous oxide semiconductors: Material design, carrier transport, and device application. *J. Non-Cryst. Solids* **2006**, *352*, 851–858. [[CrossRef](#)]
38. Martins, R.; Almeida, P.; Barquinha, P.; Pereira, L.; Pimentel, A.; Ferreira, I.; Fortunato, E. Electron transport and optical characteristics in amorphous indium zinc oxide films. *J. Non-Cryst. Solids* **2006**, *352*, 1471–1474. [[CrossRef](#)]
39. Li, G.F.; Zhou, J.; Huang, Y.W.; Yang, M.; Feng, J.H.; Zhang, Q. Indium zinc oxide semiconductor thin films deposited by dc magnetron sputtering at room temperature. *Vacuum* **2010**, *85*, 22–25. [[CrossRef](#)]
40. Kamiya, T.; Nomura, K.; Hirano, M.; Hosono, H. Electronic structure of oxygen deficient amorphous oxide semiconductor a-InGaZnO<sub>4-x</sub>: Optical analyses and first-principle calculations. *Phys. Status Solidi C* **2008**, *5*, 3098–3100. [[CrossRef](#)]
41. Leenheer, A.J.; Perkins, J.D.; van Hest, M.F.A.M.; Berry, J.J.; O’Hayre, R.P.; Ginley, D.S. General mobility and carrier concentration relationship in transparent amorphous indium zinc oxide films. *Phys. Rev. B* **2008**, *7*, 115215. [[CrossRef](#)]
42. Korner, W.; Urban, D.F.; Elsasser, C. Origin of subgap states in amorphous In-Ga-Zn-O. *J. Appl. Phys.* **2013**, *114*, 163704. [[CrossRef](#)]
43. Korner, W.; Urban, D.F.; Elsasser, C. Generic origin of subgap states in transparent amorphous semiconductor oxides illustrated for the cases of In–Zn–O and In–Sn–O. *Phys. Status Solidi A* **2015**, *212*, 1476–1481. [[CrossRef](#)]
44. Ramanauskas, R.; Iljinas, A.; Marcinauskas, L.; Milieška, M.; Kavaliauskas, Ž.; Gecevičius, G.; Čapas, V. Deposition and Application of Indium-Tin-Oxide Films for Defrosting Windscreens. *Coatings* **2022**, *12*, 670. [[CrossRef](#)]
45. Txintxurreta, J.; G-Berasategui, E.; Ortiz, R.; Hernández, O.; Mendizábal, L.; Barriga, J. Indium Tin Oxide Thin Film Deposition by Magnetron Sputtering at Room Temperature for the Manufacturing of Efficient Transparent Heaters. *Coatings* **2021**, *11*, 92. [[CrossRef](#)]
46. Mazur, M.; Obstarczyk, A.; Posadowski, W.; Domaradzki, J.; Kielczawa, S.; Wiatrowski, A.; Wojcieszak, D.; Kalisz, M.; Grobelny, M.; Szmids, J. Investigation of the Microstructure, Optical, Electrical and Nanomechanical Properties of ZnO<sub>x</sub> Thin Films Deposited by Magnetron Sputtering. *Materials* **2022**, *15*, 6551. [[CrossRef](#)] [[PubMed](#)]
47. Kim, H.-M.; Bae, K.; Sohn, S. Electronic and Optical Properties of Indium Zinc Oxide Thin Films Prepared by Using Nanopowder Target. *Jpn. J. Appl. Phys.* **2011**, *50*, 045801. [[CrossRef](#)]
48. Craciun, V.; Martin, C.; Socol, G.; Tanner, D.; Swart, H.C.; Becherescu, N.; Craciuna, D. Optical properties of amorphous indium zinc oxide thin films synthesized by pulsed laser deposition. *Appl. Surf. Sci.* **2014**, *306*, 52–55. [[CrossRef](#)]
49. Taylor, M.P.; Readey, D.W.; Teplin, C.W.; van Hest, M.F.A.M.; Alleman, J.L.; Dabney, M.S.; Gedvilas, L.M.; Keyes, B.M.; To, B.; Perkins, J.D. The electrical, optical and structural properties of In<sub>x</sub>Zn<sub>1-x</sub>O<sub>y</sub> (0 ≤ x ≤ 1) thin films by combinatorial techniques. *Meas. Sci. Technol.* **2005**, *16*, 90. [[CrossRef](#)]